Arch. Metall. Mater. **67** (2022), 2, 391-396

DOI: https://doi.org/10.24425/amm.2022.137769

M. TAGOWSKI[1*]

INFLUENCE OF 3D MODEL GEOMETRY ON DIMENSIONAL AND SHAPE CHARACTERISTICS IN ADDITIVE MANUFACTURING

Quality of 3d model in simple way translates into quality of final product, obtained from 3d printing. 3d CAx software give possibility to create enormous number of shapes – doesn't matter solids or surfaces. The question is where is the frontier between quality of 3d model and a value for money of the completed print? Is it always necessary to create as good model as possible? This paper will focus on preparation of 3d models, based on primitives and will show connection between quality of mesh, its size and deviations and quality of obtained samples, in same manufacturing conditions.

Keywords: additive manufacturing; 3d printing; 3d modelling; CAx

1. Introduction

Additive manufacturing refers to a significant number of technology types used to create prototypes. One of such technology is 3d printing using UV light-curing resins. UV curing is a photochemical process in which high-intensity ultraviolet light is used to instantly cure or dry resin in printer tank. The UV curing process is based on a photochemical reaction, using light instead of heat. Liquid monomers and oligomers are mixed with a small percentage of photoinitiators, and then exposed to UV energy [1]. Selective parts of the liquid are hardened, depending on where the light beam strikes (Fig. 1).

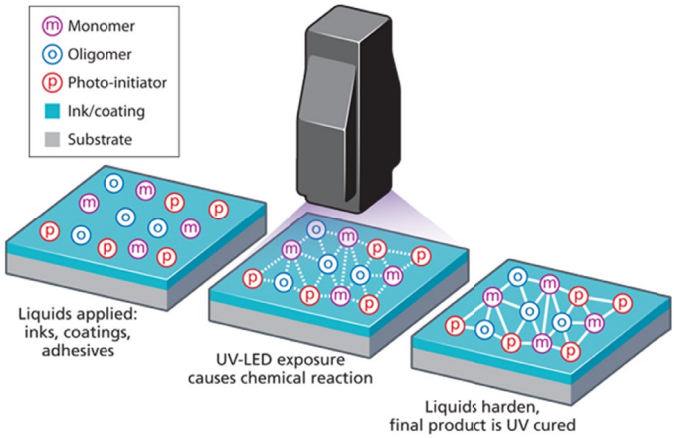

Fig. 1. Polimerization of resin in UV curing [2]

The foundations of modern 3D printing traced back to late '70s when Swainson and Kremer patented their scheme for the creation of 'Three dimensional systems'. Such system was based upon the exposure of reactive monomer systems to the intersection of radiation beams, which following a direct or indirect polymerisation process, produced a sensible 3D object or solid structure [3]. A few years later in 1980, Hideo Kodama filed a patent application for rapid prototyping. The approach was "When a liquid photo-hardening polymer is exposed to ultraviolet rays (wave length, 300-400 nm), it is solidified from the surface. The thickness of the solidified layer is a function of the UV intensity and the exposure time. Therefore, a solidified layer of the desired shape and the thickness can be grown by controlling the exposure area, intensity, and time". "Tevista" liquid photo-hardening polymer was used, which was a mixture of unsaturated polyester, acrylic ester, and styrene monomer cross-linkers, a polymerisation initiator, and a UV sensitiser. A xenon lamp (500 W) and mercury lamp (200 W) were used in top and bottom positions as well as movable base plate and xy plotter [4].

There are two main techniques in modern 3d printing, using photo-curing: SLA and DLP. The SLA as an older one is widely used in the industry. This technique was patented in 1986 by Charles Hull – the inventor of the solid imaging process and co-founder of 3D Systems, the first 3D printing company in the world [5].

[1] CZĘSTOCHOWA UNIVERSITY OF TECHNOLOGY, FACULTY OF TECHNOLOGY AND AUTOMATION, 21. ARMII KRAJOWEJ AV., 42-201 CZĘSTOCHOWA, POLAND

* Corresponding author: michalt@itm.pcz.pl

The laser light wavelength used in SLA is 355 nm. Laser head is mounted above the resin tank which is placed on a platform. This platform performs movement along vertical axis (Z axis). Each layer of the model is obtained by the downward movement of the platform and liquid resin is then solidified by the laser beam. The pattern formation of every layer is controlled by the moving of laser head. Example of such unit is presented on Fig. 2. In theory, the laser head could move over a large working area, allowing to creating large size models [6].

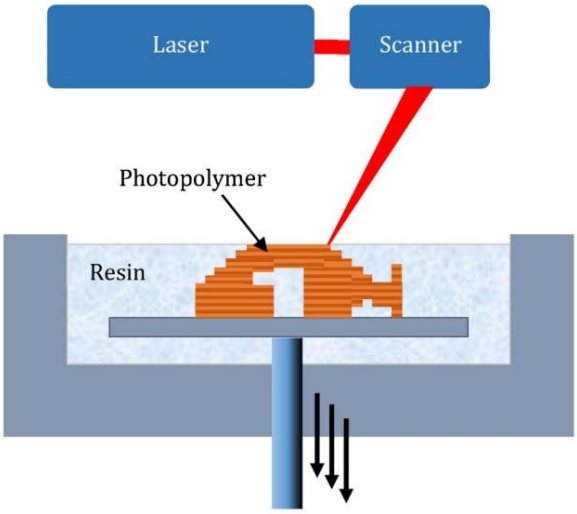

Fig. 2. SLA printing technique [7]

Main features of SLA technique:

- has low printing rate due to the curing rate depending on the moving of the laser beam. The larger size of the models, the slower the printing rate. In addition, the resins available for the cationic photopolymerization are limited.
- the printing resolution depends on the size of laser beam, thus, compared with other photocuring technique, SLA has low resolution
- the precision of SLA technique is good enough to print the objects with complex structure and fine size.
- important advantage is elimination of "trapped volume" [8]

DLP technique differs from SLA in terms of using different source of light (Fig. 3). In DLP a projector is used to project the image of the cross section of an object into photosensitive liquid resin.

It is based on invented in 1977 Digital Micromirror Device (DMD^{TM}) developed by Texas Instruments. Acting as a semiconductor light switch, the DMD can modulate incident light to produce truly digital projection display systems [10]. Three major advantages separate the DLP technology from other existing optical projection technologies. Due to its digital nature, DLP enables noise-free, precise image quality with color reproduction capabilities. DLP is better than the existing LCD technology because it is based on the reflective DMD and does not require polarized light. The million micromirrors that exist on a DMD are very closely spaced, which creates the illusion of a seamless image with greater resolution. The DMD (Fig. 4)

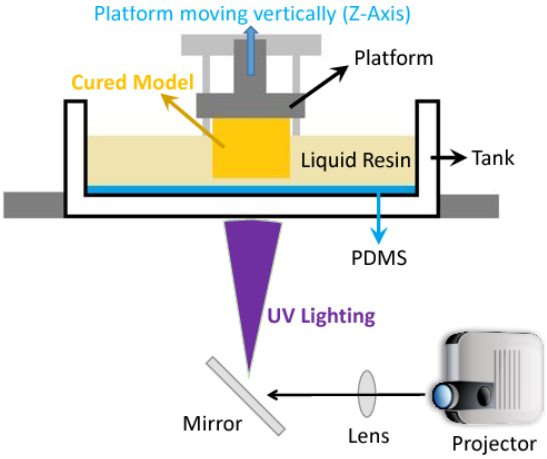

Fig. 3. DLP printing technique [9]

is basically a semiconductor light switch. It contains a million miniscule aluminum mirrors, each of which are sitting on a static random access memory cell (SRAM). Depending on the state of the underlying SRAM cell, the mirrors are able to tilt to one or another direction creating 'on' and 'off' states. The tilting capability of the mirrors, combined with the light source and the optics provide the DMD™ with the ability to project or restrict light on a particular area of the projected surface [11].

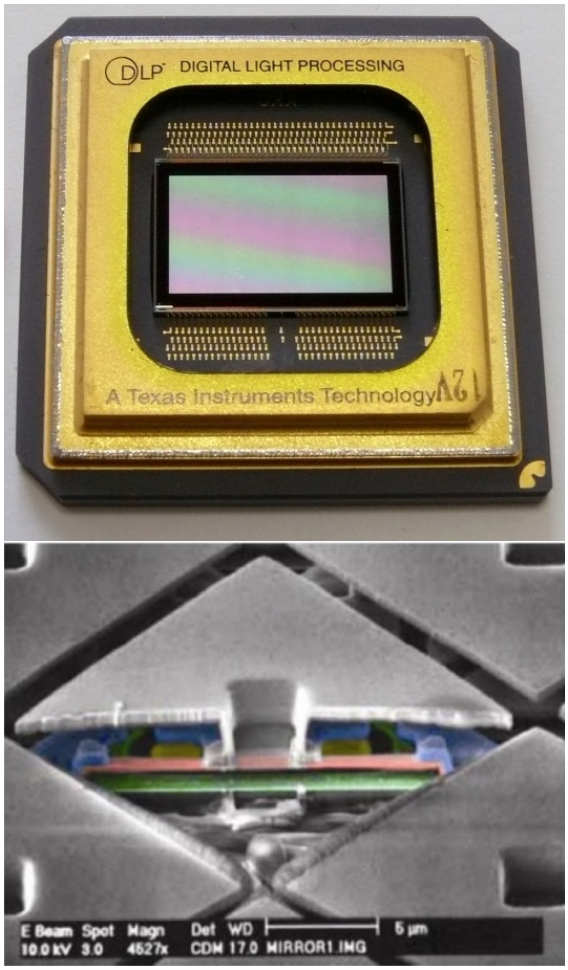

Fig. 4. DLP Chip (top) [Texas Instruments] cross section of DMD (bottom) [12]

In normal exploitation, the free radical photosensitive resin is used for DLP technique. There are two reasons why do not use cationic photopolymerization. The first reason – cationic photoinitiator could hardly work under 405 nm irradiation. There are cationic photoinitiator which could work under 405 nm, however, it`s too expensive to use it commonly. The second, the intensity of the light in DLP printing isn't high enough to photolysis the cationic photoinitiators, which can't induce the photopolymerization [6].

Main features of DLP technique:

- the biggest advantage of DLP technique is high precision of printing (difference between SLA and DLP prints quality is presented on Fig. 5)
- it could only print the model with small size, thus, it is mainly used in the fields of jewelry casting and dentistry

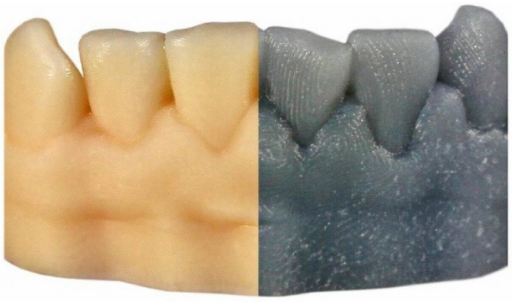

Fig. 5. Comparison of printing final result of DLP (left) and SLA (right) technique [13]

2. Preparations of 3d models

In meshing techniques the concept of element size is self-explanatory. A smaller element size leads to more accurate results at the expense of a larger computation time. The "sag" terminology is unique to CATIA. During tesselation, the geometry of a part is approximated with the elements. The surfaces of the designed part and the numerical approximation of such part do not coincide. The "sag" parameter controls the deviation between the two. Therefore, a smaller "sag" value could lead to better results. [14] So the sag value is the maximum distance between the geometry and the triangles, and the step value controls the length of triangles. The sizes of the "step" and "sag" on the screen, which also limit the coarseness of the mesh, can be changed by the user, during tessellation definition.

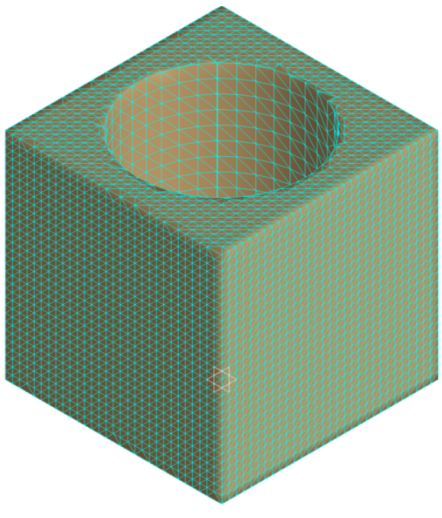

Fig. 6. Defined mesh of the test sample

The test models were cubes with dimensions: 30×30×30, with hole placed in the center, of diameter 23 mm. Then meshes were prepared with different step (St) and sag (S) values (Fig. 6 and parameters according to TABLE 1).

TABLE 1

Specimen	No. of vertices	No. of triangles
St1S1, St1S5, St1S10	123 984	41 328
St5S1, St5S5, St5S10	5 124	1 708
St10S1, St10S5, St10S10	1 380	460

Fig. 7. presents example of the group, in which samples varies by the value of the step parameter with constant sag, equal to 1 mm.

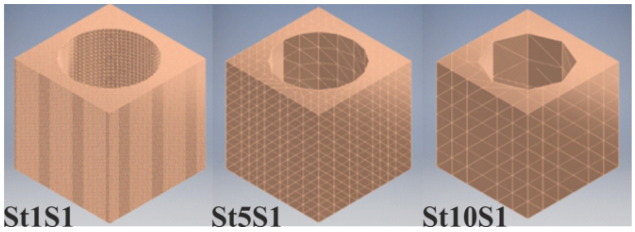

Fig. 7. The view of the meshes with constant sag value and different step

3D Prints were taken on the RapidShape D20 II printer. It is compact unit dedicated for medical practices, clinics, and small labs. TABLE 2 presents brief description of basic parameters.

TABLE 2 [15]

Building area	133×75 mm
Native pixel	±34 µm
Max. part height	90 mm
Light source	385 nm UV LED
Resolution	1920×1080 px

The resin DREVE FotoDent® model2, which was used to print the test models was based on methacrylate resin for DLP systems with 385 nm LED for the manufacturing of dental models. Mechanical properties of resin are: Density approx. 1.1 g/cm³, Viscosity (295,93 K) 1 ±0.2 Pa s, Flexural modulus ≥1900 MPa, Flexural strength ≥85 MPa, Elongation at break ≥8%

3. Preliminary measurements and its results

Each detail was printed separately under the same conditions, with separate lamp calibration before each printing. The controlling code for printer was prepared in Netfabb. After print-

ing each model was cleaned in ultrasonic cleaner in isopropanol bath, and after that each sample was curing for 5 minutes inside 360deg UV curing chamber. The final effect of above treatment is shown on Fig. 8. Numbers on the top plane of each model, describes the measuring base both in preliminary measurements, which exclude possible greatest deviations, as well as in main measurements.

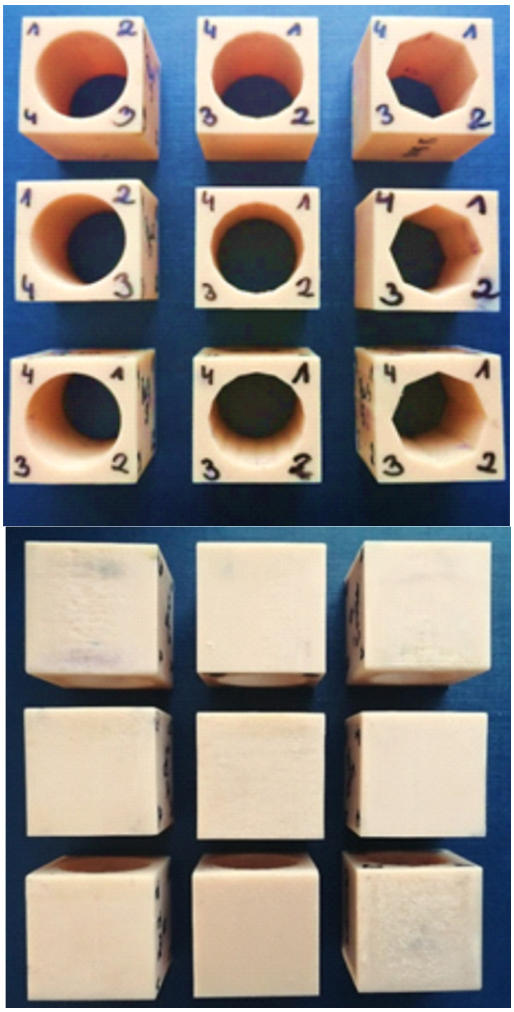

Fig. 8. Set of printed models

Preliminary measurements were performed using digital caliper and vertical length measuring machine. Caliper measurements were taken in three cross sections of the measured cube. Fifteen measurements were taken on each surface: five measurements over three sections. Measurements using length meter were also made in three sections. The face with the cylindrical cut out was measured at four points five times each. The other two surfaces were measured at five points (including point at the intersection of diagonals), also five times each. Example of the preliminary measurements of a sample St1S1 are shown in TABLE 3. Actual dimensions of sample St1S1 are shown on Fig. 9.

For dimensions obtained during measurements with a caliper and a length meter, the following statistical tests were carried out: Dixon test, Grubbs test and the test of significance. After performing the Dixon test, it was observed for all samples that no measurement was subjected to a disqualyfying error ($\alpha = 95\%$). Grubbs test pointed four measurements, which were flawed – that measurements were removed from an analysis. After performing the significance test, it was observed that no result was in the critical area. Therefore, there is no reason to reject the H_0 hypothesis (sample is not affected by an error and it does not affect the arithmetic mean of the population).

TABLE 3

St1S1	Arithm. mean $\bar{x}$ for section	Std. Dev. $s(x)$ for section	Std. Err. $s(\bar{x})$ for section	Arithm. mean $\bar{x}$ for surface	Std. Dev. $s(x)$ for surface	Std. Err. $s(\bar{x})$ for surface
Caliper						
Z axis (sec. 1)	30,084	0,015	0,007	30,076	0,018	0,005
	30,068	0,013	0,006			
	30,076	0,022	0,010			
Y axis (sec. 2)	30,228	0,033	0,015	30,231	0,031	0,008
	30,216	0,026	0,012			
	30,250	0,023	0,010			
X axis (sec. 3)	30,112	0,023	0,010	30,229	0,149	0,038
	30,436	0,014	0,006			
	30,138	0,033	0,015			
Vertical length measuring machine						
Z axis (surf. 1, hole)	30,098	0,015	0,007	30,087	0,013	0,003
	30,070	0,002	0,001			
	30,085	0,003	0,001			
	30,094	0,001	0,001			
Y axis (surf. 2)	30,165	0,065	0,029	30,153	0,079	0,016
	30,127	0,007	0,003			
	30,117	0,007	0,003			
	30,073	0,003	0,001			
	30,285	0,032	0,014			
X axis (surf. 3)	30,192	0,020	0,009	30,253	0,096	0,019
	30,284	0,031	0,014			
	30,187	0,011	0,005			
	30,183	0,063	0,028			
	30,417	0,016	0,007			

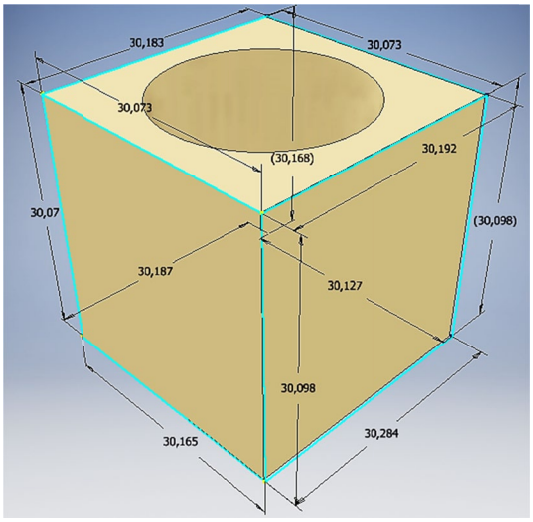

Fig. 9. Actual dimensions of the sample St1S1

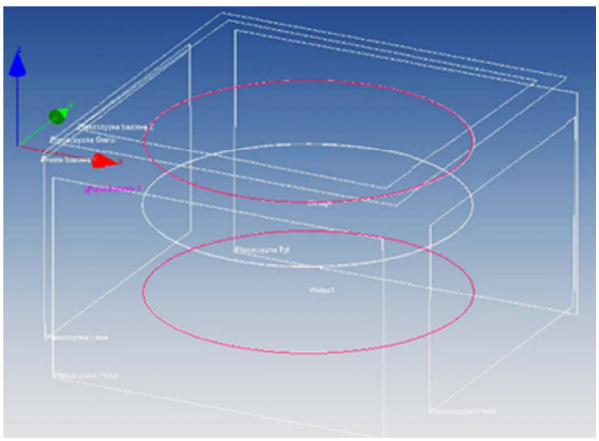

Fig. 10. CMM measurement strategy

4. CMM measurements

CMM measurements were performed on Zeiss Eclipse 700 with Calypso software. The whole measurement strategy (Fig. 10) covered below features: one hundred measurement points were collected for the lateral planes (each), 36 points were collected for cylinder, at seven levels every two mm. (starting about 3 mm below the top plane of the measured cube), while 60 measuring points were collected, checking roundness on the half-height plane. Measurement time for a single sample was 42 minutes.

Sought geometrical parameters were parallelism and perpendicularity of the side walls, hole cylindricity and roundness. Fig. 11 and 12 shows few examples of comparison between the worst and the best obtained results, inside the whole group of samples.

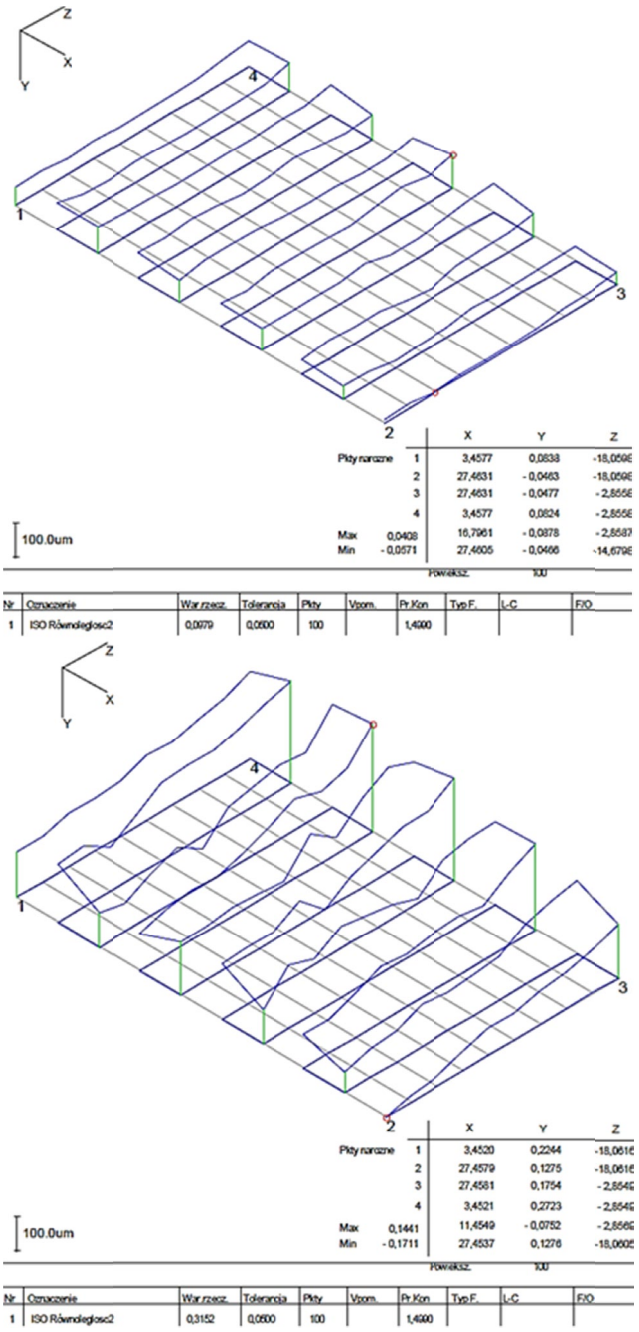

Fig. 11. Parallelism for St10S1 (top) and St10S10 (bottom)

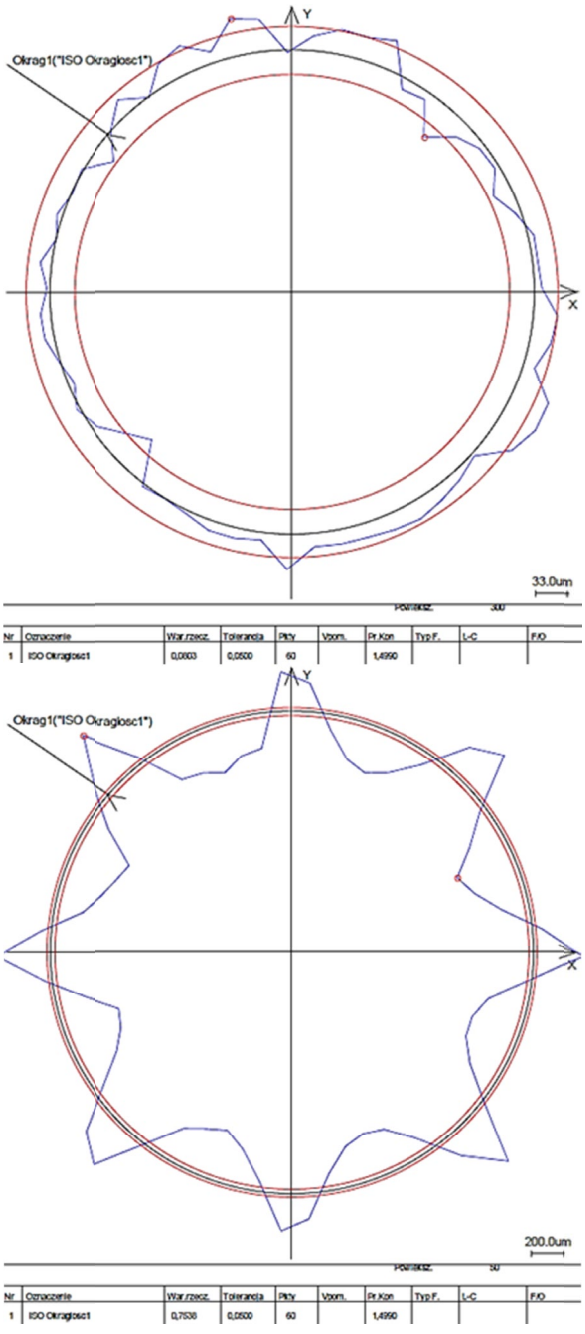

Fig. 12. Roundness for St10S1 (top) St10S10 (bottom)

5. Conclusions

The St10S10 sample had by far the largest deviations. Its surface smoothness (visually) as well as dimensions indicate a low manufacturing accuracy. Samples St10S1 and St10S5 were distinguished by a high value of roundness and cylindrical deviation and the values of parallelism and perpendicularity deviation were better compared to St10S10. The dimensional values were not satisfactory, but the smoothness of the surface of the walls, compared to the walls of the rest of the samples, was the smoothest. The St5S1 sample, despite having better roundness and cylindrical deviation values, was characterized by a high perpendicularity deviation value. St1S1 had average deviation values and the effects of the thermal shrinkage of the resin were visible on the surface of the cube. St1S1, however, was distinguished by the closest dimension to the nominal value in the z axis. The St1S5 cube was characterized by low values of shape error, good dimensional properties, but the wall surfaces of the model were not the best. Compared to others, the St5S5 element was distinguished by quite good dimensions in each of the axes and satisfactory values of shape errors. Unfortunately, furrows were visible on the surface of this ankle. Among all samples, the smallest values of shape errors were characterized by samples St5S10 and St1S10. Still, the dimensional characteristics were not the best (according to Fig. 13).

As observed low step value increases dimensional accuracy but not so significant in comparison to average value (step = 5 mm). Sag parameter affects the accuracy of the shape. For cubic samples both of this parameters are sufficient in the average values of the assumed range.

It is worth asking the question: can the nature of the deviations obtained in the presented models (produced with SLA / DLP methods) be considered binding for the entire group of details, created with additive methods? Particular attention should be paid to the Selective Laser Melting (SLM) and Direct Metal Laser Sintering (DMLS) methods. Due to the completely different characteristics of the material (metal powders), it seems that the answer should be negative, however, the research will be continued.

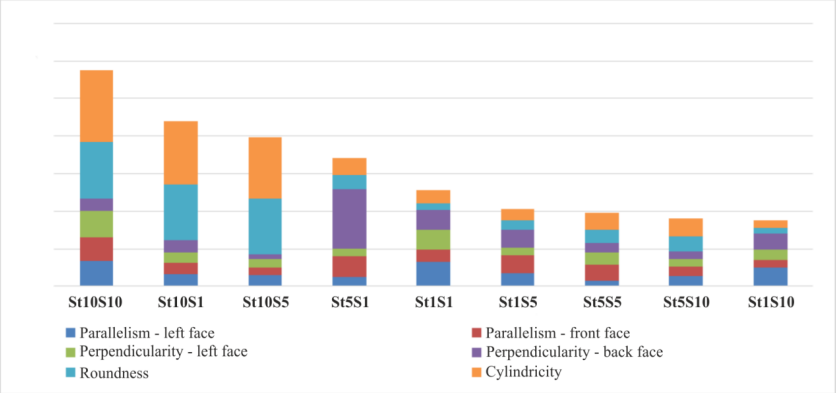

Fig. 13. Cumulative comparison of deviations in the whole group of samples

REFERENCES

[1] https://www.alpha-cure.com/(accessed: 10 05 2020).

[2] https://rimotec.nl/uv-curing/ (accessed: 12 05 2020).

[3] V. Gupta, P. Nesterenko, B. Paull, 3D Printing in Chemical Sciences: Applications Across Chemistry, Royal Society of Chemistry, (2019). DOI: https://doi.org/10.1039/9781788015745

[4] H. Kodama, Automatic method for fabricating a three-dimensional plastic model with photo-hardening polymer, Review of Scientific Instruments **52**, 1770-1773 (1981). DOI: https://doi.org/10.1063/1.1136492

[5] https://www.3dsystems.com/our-story (accessed: 14 05 2020).

[6] H. Quan, T. Zhang, H. Xu, S. Luo, J. Nie, X. Zhu, Photo-curing 3D printing technique and its challenges, Bioactive Materials **5**, (1), 110-115 (March 2020). DOI: https://doi.org/10.1016/j.bioactmat.2019.12.003

[7] G.A. Appuhamillage, MSc New 3D printable polymeric materials for fused filament fabrication (FFF), Virginia Polytechnic Institute and State University, (2018). DOI: https://doi.org/10.13140/RG.2.2.31264.43526

[8] D.T. Pham, S.S. Dimov, Rapid Manufacturing. The technologies and applications of rapid prototyping and rapid tooling, 2011 Springer, London.

[9] C. Wu, R. Yi, Y-J. Liu, Y. He, C. C.L. Wang, Delta DLP 3D printing with large size, 2155-2160, IEEE/RSJ International Conference on Intelligent Robots and Systems (IROS), (2016). DOI: https://doi.org/10.1109/IROS.2016.7759338

[10] J.M. Florence, L.A. Yoder, Display system architectures for digital micromirror device (DMD)-based projectors, 193-216, Proc. SPIE 2650, Projection Displays II, (29 March 1996). DOI: https://doi.org/10.1117/12.237004

[11] R.M. Mainur, MSc, Statistical analysis of the digital micromirror devices hinge sag phenomenon, Texas Tech University, (05-2002).

[12] Z. Zhou, Z. Wang, L. Lin, Microsystems and Nanotechnology, Springer Science & Business Media, (2012).

[13] Advanced DLP for superior 3d printing, envisiontec.com (accessed: 15 05 2020).

[14] N. Zamani, CATIA V5 FEA Tutorials Release 20, SDC Publications, (March 21 2011).

[15] www.rapidshape.de/Datasheet_D20 (accessed: 24 02 2020).